AD 270 852

NAVWEPS REPORT 7758
NOTS TP 2728
COPY 56

STRESS-CONCENTRATION DATA FOR INTERNALLY PERFORATED STAR GRAINS

by
M. E. Fourney
and
R. R. Parmerter
Mathematical Sciences Corporation

ABSTRACT. Completing preliminary work initiated by NOTS several years ago, photoelastic tests were conducted to determine the maximum tangential stress for a family of star-grain configurations in a state of plane stress. Curves are presented that give the value of the ratio of tangential stress to external pressure for web fractions from 20 to 60%, for w/ρ from approximately 2 to 30 (w is the web thickness of the grain, and ρ is the radius of the star point), and for N (number of star points) from 3 to 8. The accuracy of the curves is estimated to be within $\pm 4\%$. The effect of the inverse star point was investigated and found to be negligible over a range of shapes and values of the parameter a'/a (ratio of distances from center to the inverse star point and to the outer star point) from approximately zero to 0.6. The experimental results compared favorably with one theoretical calculation. Equations are given for extension of the data to case-bonded, internally pressurized grains and for application to problems of tangential strain. An appendix presents an empirical equation representing the data.

U. S. NAVAL ORDNANCE TEST STATION
China Lake, California
December 1961

U. S. NAVAL ORDNANCE TEST STATION

AN ACTIVITY OF THE BUREAU OF NAVAL WEAPONS

C. BLENMAN, JR., CAPT., USN
Commander

WM. B. McLEAN, PH.D.
Technical Director

FOREWORD

Some preliminary design data for stresses in star grains were developed several years ago by the use of photoelastic techniques. Because of the importance stress analysis has assumed in the development of current and proposed propulsion systems, and because the purely theoretical approach has not as yet developed into a useful engineering tool, extension of the earlier work was deemed desirable. This report presents the results of the additional work, which increased the number of parameters and improved the accuracy of the results.

The work was performed for the U. S. Naval Ordnance Test Station by the Mathematical Sciences Corporation (formerly Southwest Engineers) under Contract No. N123(60530)25914A during the period November 1960 to May 1961.

This report was reviewed for technical accuracy by K. H. Bischel and W. W. Oshel.

Released by
C. M. HAVLIK, *Head,*
Process Development Div.
11 July 1961

Under authority of
J. T. BARTLING, *Head,*
Propulsion Development Dept.

NOTS Technical Publication 2728
NAVWEPS Report 7758

Published by ..... Publishing Division
Technical Information Department
Collation ..... Cover, 13 leaves, abstract cards
First printing ..... 220 numbered copies
Security classification ..... UNCLASSIFIED

CONTENTS

Nomenclature iv
Introduction 1
Statement of Problem To Be Considered 1
Calibration Tests 3
Star-Configuration Tests 7
Effect of the Inverse Star Point 11
Processing of Test Data 11
Error in Experimental Results 13
Comparison With a Theoretical Solution 15
Extension of Test Data 15
Stress-Concentration Factors 15
Strain-Concentration Factors 18
Conclusions 19
Appendix 20
References 23

NOMENCLATURE

a	Radius to outer star point, in.
a'	Radius to inverse star point, in.
A	Inverse-star point
b	Radius of grain, in.
d	Differential
D	Diameter of grain, in.
E	Young's modulus
f	Stress-optic constant
F	Fringe constant based on $h = 0.250$ in.
G	Shear modulus
h	Thickness of model, in.
K_i	Stress-concentration factor at the inner surface of the grain
L	Load, lb
n	Isochromatic fringe order
N	Number of star points
p_g	Gage pressure
p_i	Internal pressure
p_0	External pressure
p'	Pressure at interface of grain and case
P	Ratio of interface pressure to internal pressure
w	Web thickness of grain, in.
γ	Shear strain
ϵ	Strain
ν	Poisson's ratio
ρ	Radius of star point
σ	Stress
τ	Shear stress

SUBSCRIPTS

c	Pertaining to grain case
g	Gage
i	Internal
r	Radial
z	In a direction normal to the plane of the slice
θ	Circumferential

INTRODUCTION

The extensive use of large solid-propellant rockets in recent years has intensified the need for more precise methods of stress analysis of such systems. The complete stress analysis, which is but a part of the real task of determining the structural integrity of the system, is in itself an exceedingly difficult problem. This report is concerned with a very limited aspect of the general problem and deals specifically with the stress and strain concentrations that exist at the star points of a long, tubular solid-propellant grain subjected to internal pressure. The report amplifies certain preliminary data obtained by Southwest Engineers for the U. S. Naval Ordnance Test Station in an earlier study (Ref. 1), which provided the first parametric investigation of structural implications induced by ballistic changes in the charge. Because of the unusual and irregular shapes of rocket-grain cross sections, it is usually impractical to employ analytical stress-analysis methods, and hence alternate techniques become attractive.

Following the previous investigation, a photoelastic approach was used to improve the accuracy of the preliminary data and extend the applications pointed out by Ordahl and Williams (Ref. 1). The tests to be discussed concentrate upon a family of star grains and present stress-concentration data believed to be accurate within ±4% over the range of design interest.

STATEMENT OF PROBLEM TO BE CONSIDERED

The structural integrity of solid-propellant grains is a problem that has received much attention in the past several years (Ref. 2). The major difficulties are due to the need for a viscoelastic analysis and the lack of an adequate failure criterion. Advances in both areas are hampered by the complicated grain geometry. It is the aim of this report to present one set of data showing the effect of the geometry on the magnitude of the maximum stress caused by a pressure loading. While the analysis applies specifically to an elastic body, it may be shown (Ref. 2) that for cases where the boundary conditions are imposed essentially in terms of stresses, the viscoelastic and elastic stress distributions are identical. Hence, for engineering purposes it is found that the viscoelastic stress distribution in the cross section of a long tubular grain may be obtained by photoelastic studies.

Photoelastic experiments are conducted on thin slices for which plane-stress assumptions are used, i.e., the stress normal to the slice, σ_z, is taken to be zero. These data are analytically transferable to a long-tube grain where the axial strain, ϵ_z, is either zero or constant. This is therefore the condition to which the data will apply; specifically, they are not expected to apply near the ends of the grain or near abrupt changes in cross section such as at a head- or after-end closure.

It should also be stated that the rocket grain is assumed to be composed of an isotropic, homogeneous continuum, notwithstanding the presence of filler particles and possible voids in the viscoelastic binder of the propellant.

The geometry of the specific family of cross sections to be tested is shown in Fig. 1. The maximum stress, as shown in Fig. 2 by the concentration of the photoelastic fringes around each star point, occurs at the star point, which lies along a radial line where the shear stress, $\tau_{r\theta}$, is

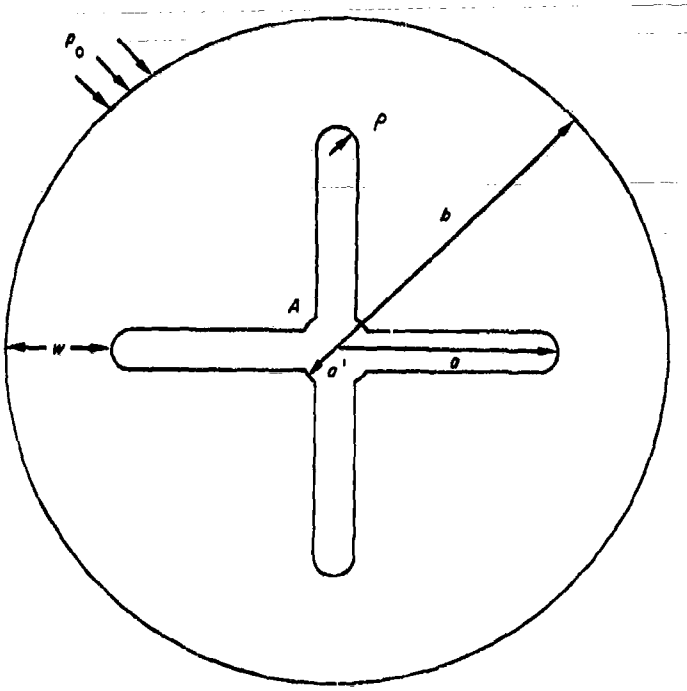

FIG. 1. Geometry of Cross Section of a Star Grain. ρ, radius of star point; b, radius of grain; a, radius to outer star point; a', radius to inverse star point; w, web thickness; A, inverse star point; p_0, external pressure.

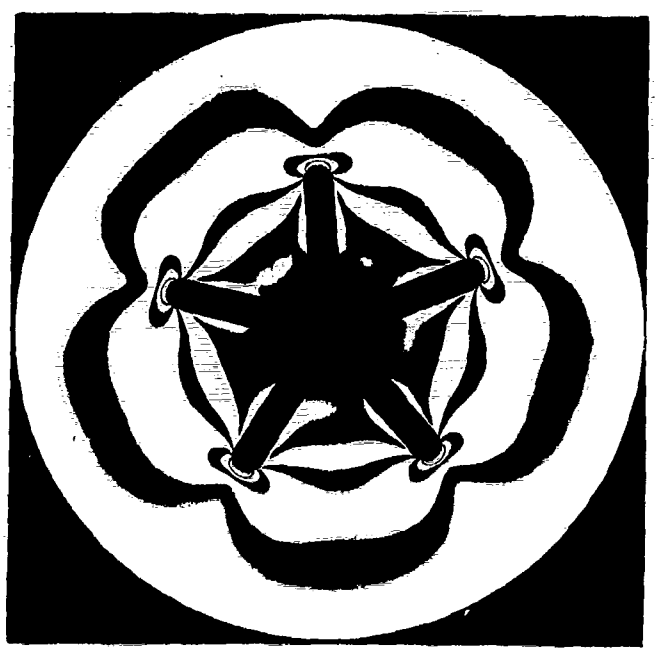

FIG. 2. Five-Point-Star Grain Subjected to External Pressure.

zero by symmetry. Hence, the radial and circumferential stresses, σ_r and σ_θ, respectively, are the principal stresses that permit immediate application of the fundamental stress-optic law

$$\sigma_1 - \sigma_2 = 2fn/h \tag{1}$$

where

$\sigma_{1,2}$ = the principal stresses
f = stress-optic constant for the material used in the test
h = thickness of model
n = isochromatic fringe order

Inasmuch as the radius equals a at the internal boundary, the radial stress, σ_r (or denoting it by the principal stress, say σ_2), will always be known: $\sigma_r = -p_i$ if loaded by internal pressure, or $\sigma_r = 0$ if unloaded. The maximum (circumferential) stress, σ_θ (or σ_1), will be completely determined from Eq. 1 as

$$\sigma_\theta = 2fn/h + \sigma_r \quad \text{(at the star point)}$$

providing the fringe order, n, and the model characteristics are known. For zero internal pressure, this can be written in an equivalent form as[1]

$$\frac{\sigma_\theta}{p_0} = \frac{2f/h}{dp_0/dn} \tag{2}$$

In the problem of practical interest, that is, a rocket motor subjected to internal pressurization, the grain is subjected to both an internal and an external pressure imposed by the rigidity of the case. As will be discussed later, these continuity and displacement conditions at the case are simulated by an equivalent, uniform interface pressure, which is sufficiently accurate for most engineering purposes. With this approximation, the important parameter in determining the stress distribution by photoelastic means is only the pressure difference across the web (Ref. 1), and it may be shown[2] that the fringe pattern is a function only of this difference.

CALIBRATION TESTS

For the calibration tests, it was necessary to determine the relationship between fringe order and stress. Also, since the specimen was to be loaded by a uniform pressure applied to the outer circumference, it was necessary to calibrate the loading device. The device, based upon that used earlier (Ref. 1), applied air pressure through a rubber diaphragm to the specimen. Thus, the relationship between air pressure indicated in a gage (p_g) and the pressure applied to the specimen (p_0) was required.

The fringe constant was determined by loading several disks of various diameters with two equal diametral loads (Fig. 3). The load required to produce 1, 2, ···, 8 fringes at the center of each disk was noted, and the slope of the straight line through the eight data points, dL/dn, was determined. The theoretical solution for this loading is

[1] For a linear system, the stress is proportional to the applied pressure, hence $\sigma_\theta/p_0 = d\sigma_\theta/dp_0 = (2f/h)(dn/dp_0)$ under the assumption that at zero pressure, the grain is stress-free.

[2] A uniform pressure, p, applied to both inner and outer boundaries of any multiply connected, two-dimensional region results in a state of hydrostatic stress: i.e., $\sigma_r = \sigma_\theta = -p$, so the resultant fringe order, which depends on $\sigma_r - \sigma_\theta$, is always zero. Thus, this state may be superimposed on any given state without altering the fringe pattern. A problem with p_i internal and p_0 external pressure may be converted to a problem with $p_i - p_i = 0$ internal pressure and $p_0 - p_i$ external pressure without changing the fringe pattern. Hence, the fringe pattern depends only on $p_0 - p_i$.

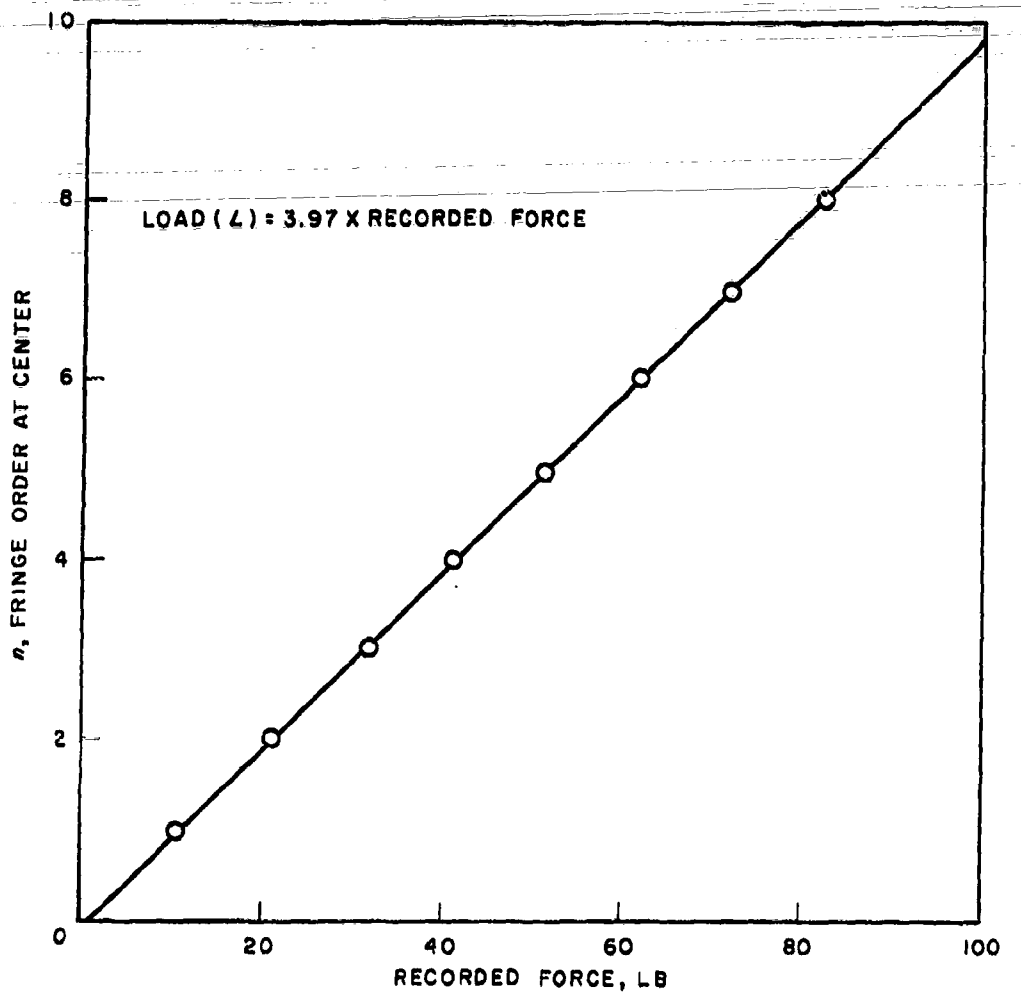

FIG. 3. Typical Slope for the Determination of Fringe Constant for CR-39 Plastic Disk.

$$\frac{dL}{d(\sigma_1 - \sigma_2)} = \frac{\pi h D}{8} \tag{3}$$

where L is the load, h the thickness, D the diameter, and $\sigma_1 - \sigma_2$ is the difference in principal stress. Thus, the value of $2f/h = F$ in the stress-optic law (Eq. 1) $\sigma_1 - \sigma_2 = Fn$ can be computed for

$$F = \frac{8(dL/dn)}{\pi h D}$$

Assuming F to be constant, Eq. 3 becomes

$$\frac{dL}{dn} = \frac{\pi h F}{8} D \tag{4}$$

The average value obtained from the tests was $F = 333$ psi per fringe, based on a specimen thickness $h = 0.250$ inch. Taking the value of F to be 333, the test points can be compared to the theoretical value. This comparison is shown in Fig. 4, and reveals only a small scatter of data.

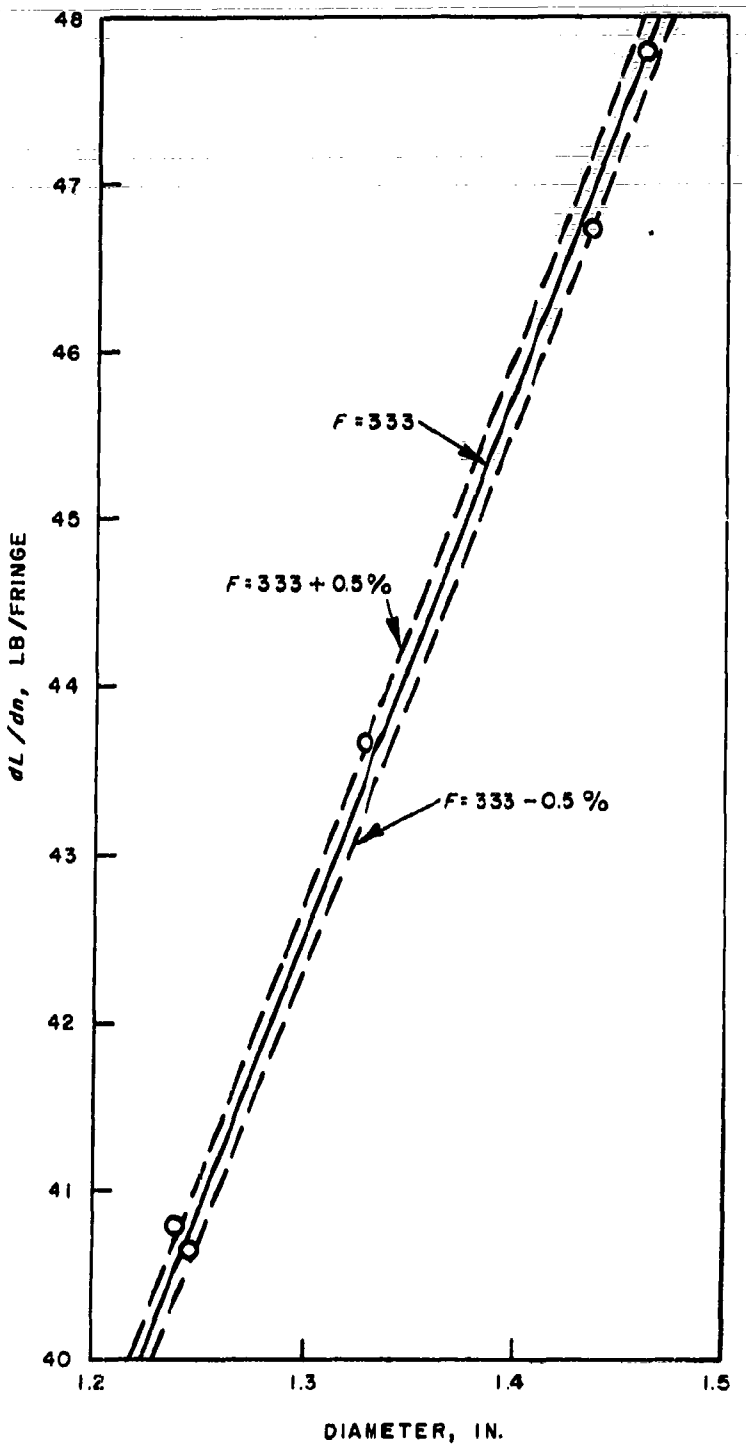

FIG. 4. Comparison of Theoretical and Experimental Relationships of Load-to-Fringe Ratio With Diameter of Diametrally Loaded CR-39 Plastic Disks.

A series of thick-walled hollow cylinders was tested next in the pressure-loading jig to determine the relationship between p_g and p_0. It was found that $p_g/p_0 = 1$; hence, no further distinction was made between these subscripts. The difference in principal stress in a thick-walled hollow cylinder at the inner wall under external pressure loading, p_0, is given by

$$\frac{d(\sigma_1 - \sigma_2)}{dp_0} = \frac{2}{1 - (a/b)^2} \tag{5}$$

Assuming $F = 333$, dp_0/dn was calculated from the test data and compared to the theoretical value in Fig. 5. It should be noted that the data fall within the ±5% band.

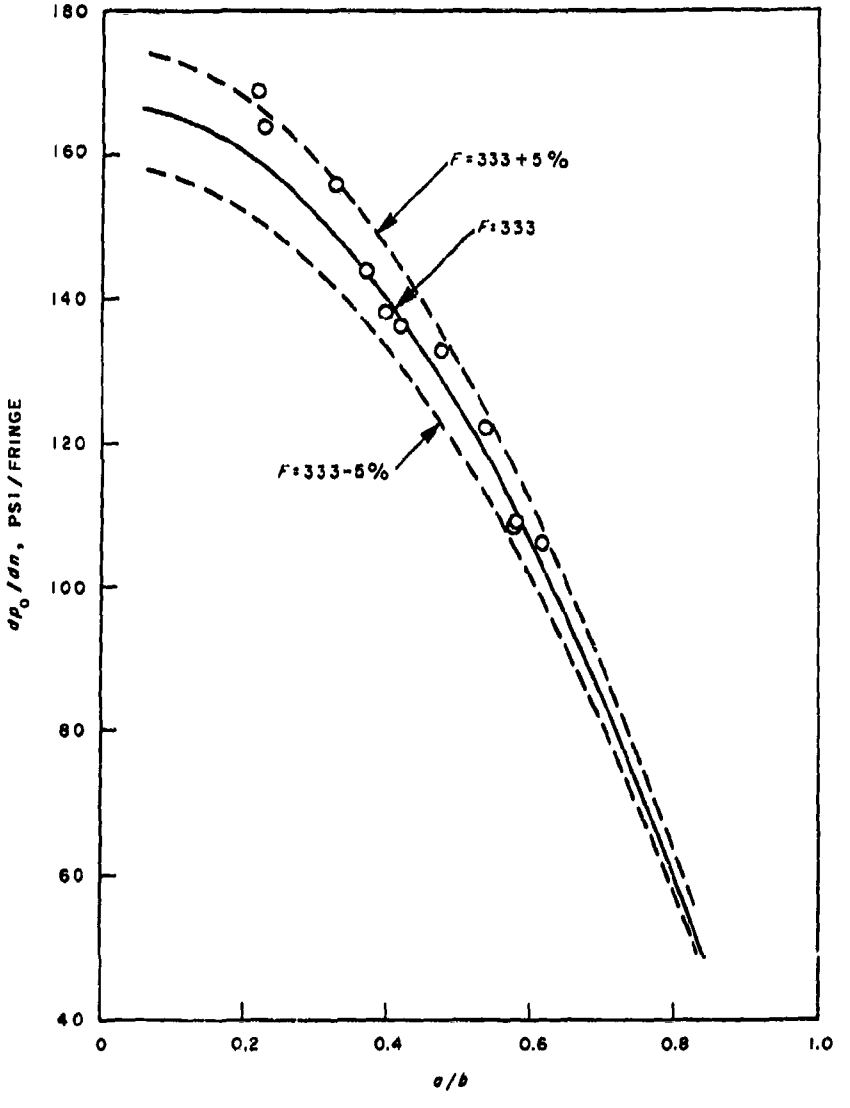

FIG. 5. Comparison of Theoretical and Experimental Relationships of Pressure-to-Fringe Ratio With a/b for an Externally Pressurized Thick-Walled Hollow Cylinder.

STAR-CONFIGURATION TESTS

The grain configurations tested for this report were all of the type shown in Fig. 1. It is clear that the configuration is completely specified by the nondimensional parameters w/b, w/ρ, a'/a, and N, where $w = b - a$, and that the stress pattern and nondimensional ratios such as σ_θ/p_0 are independent of the specific magnitude of b. For the specimens tested, $b = 5.480$ inches, and $a'/a = 0.137$. The dependence of σ_θ/p_0 on w/b, w/ρ, and N is presented in Fig. 6–10. An empirical equation representing the data appears in the Appendix. The dependence of σ_θ/p_0 on a'/a was investigated for two configurations, and σ_θ/p_0 was found to be nearly independent of this parameter for values of a'/a up to 0.6. These results are presented in Fig. 11.

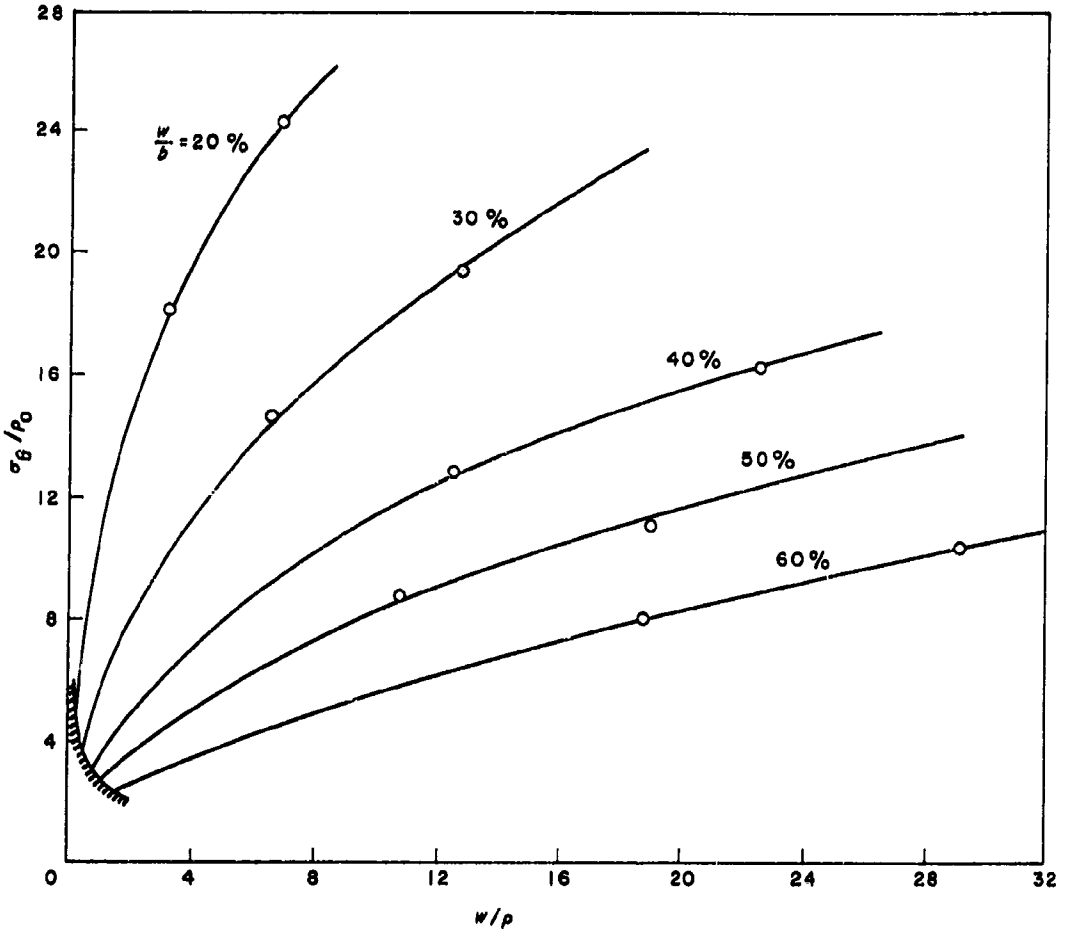

FIG. 6. Effect of Grain-Dimension Parameters on the Stress at the Star Point of an Externally Pressurized Three-Point-Star Grain.

The specimens to be tested were machined from CR-39 plastic on a milling machine. The procedure was such that the dimensions of the star configuration were held within ±0.005 inch, and the angular position of the star points was held within ±5 minutes of arc. These tolerances

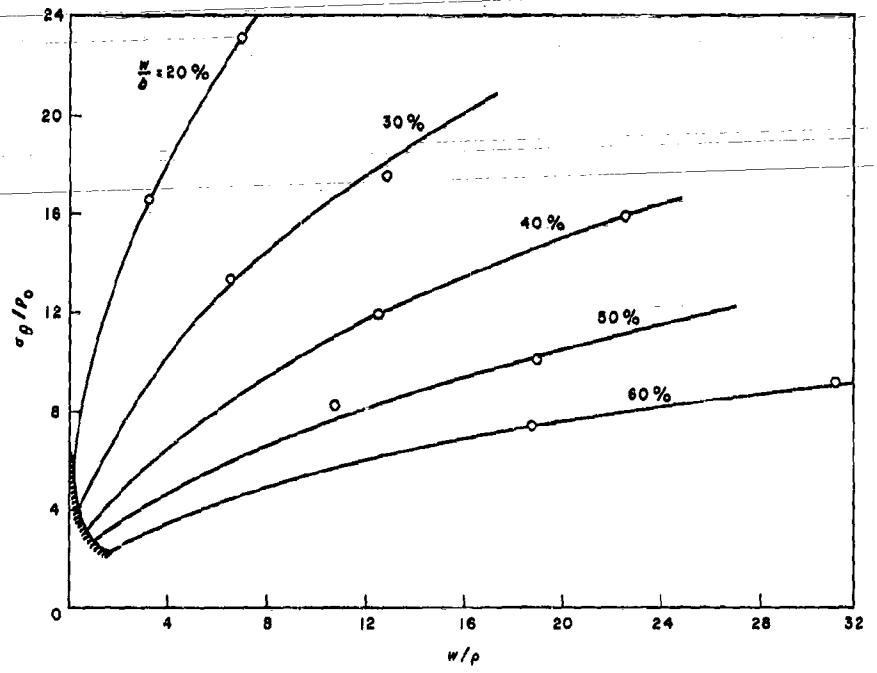

FIG. 7. Effect of Grain-Dimension Parameters on the Stress at the Star Point of an Externally Pressurized Four-Point-Star Grain.

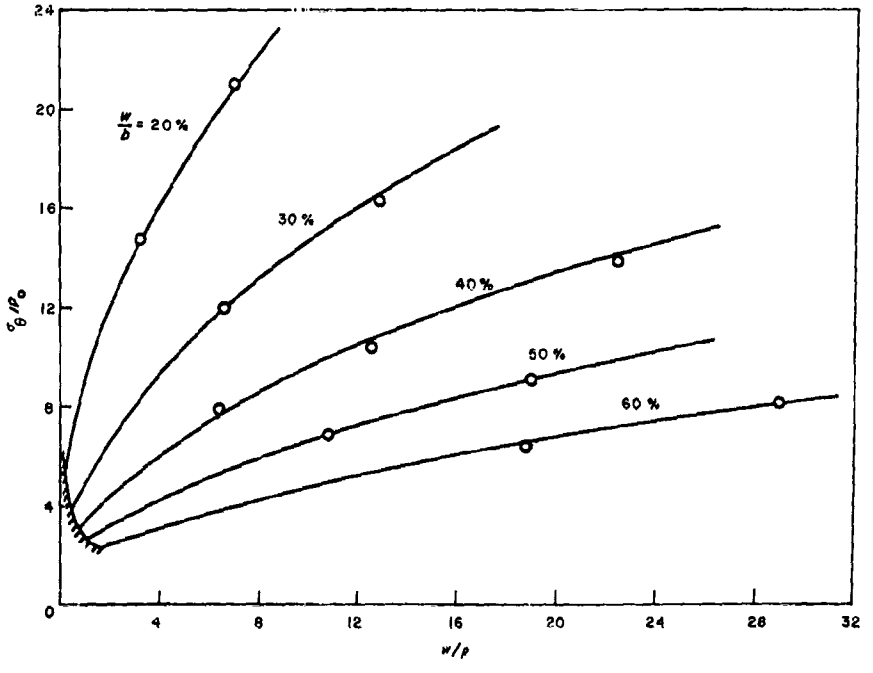

FIG. 8. Effect of Grain-Dimension Parameters on the Stress at the Star Point of an Externally Pressurized Five-Point-Star Grain.

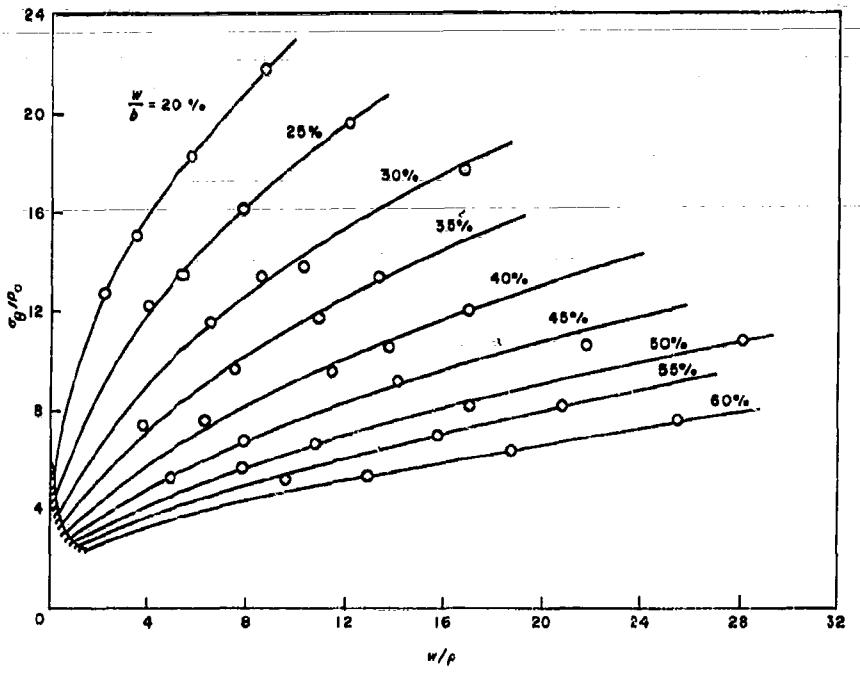

FIG. 9. Effect of Grain-Dimension Parameters on the Stress at the Star Point of an Externally Pressurized Six-Point-Star Grain.

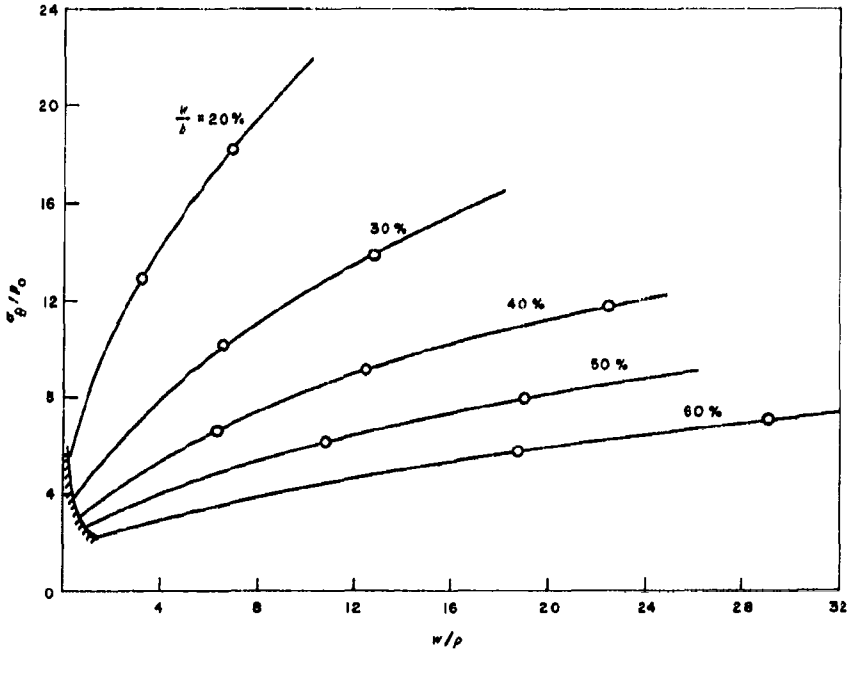

FIG. 10. Effect of Grain-Dimension Parameters on the Stress at the Star Point of an Externally Pressurized Eight-Point-Star Grain.

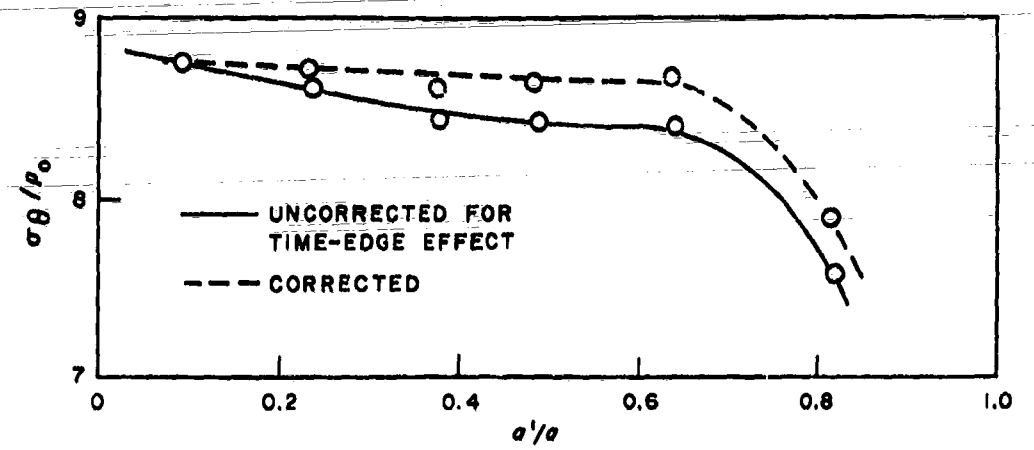

(a) Three-point-star grain.

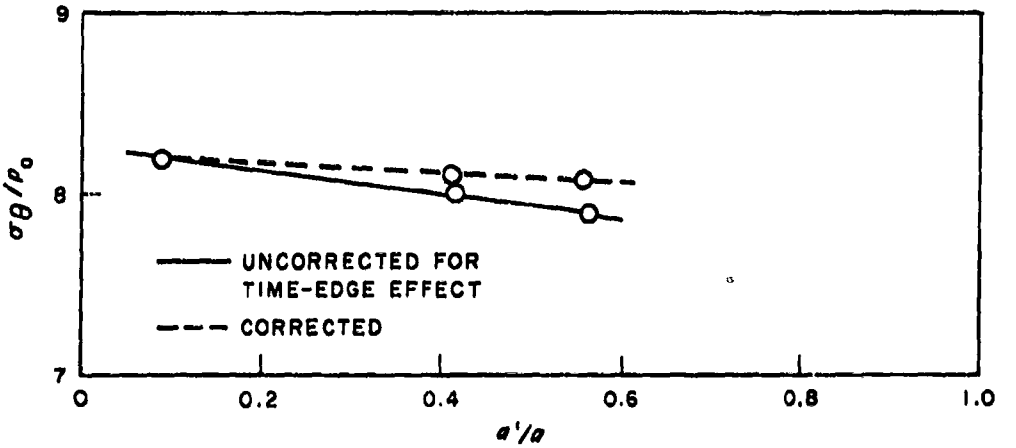

(b) Four-point-star grain.

FIG. 11. Effect of Inverse Star Point on the Stress at the Star Point; $a/b = 0.5$; $w/\rho = 10.79$.

are more than enough to ensure that any errors in the final result arising from inaccurate geometry are completely negligible compared to other errors inherent in the method.

CR-39 exhibits a time-edge effect that tends to obscure and distort the fringes near the edge of a specimen when it is allowed to stand after machining. A lapse of over an hour is enough time to hamper severely a photoelastic determination of edge stresses; therefore, each configuration was tested immediately after machining. By widening and extending the star point at each step, it is possible to obtain several specimens cut to different configurations from one blank, while producing a fresh edge to minimize time-edge effect at each step. In this way, from three to seven test points may be obtained from each blank.

As a control, each blank was first machined to a thick-walled cylinder configuration with an inside diameter of 0.375 inch (corresponding to $a/b \approx 0.137$) and pressure-tested. After completion of the parametric changes of star-configuration tests on a given blank, the remainder was again cut into a thick-walled cylinder and tested. These two tests of a configuration whose

stresses could be analyzed theoretically gave two check points on each blank. In addition, a small disk was cut from the remains of each blank and tested by applying a diametral load as previously described. Since the two loading rigs were different, this procedure provided an independent check of the fringe constant for each blank.

EFFECT OF THE INVERSE STAR POINT

Another series of tests was run to determine the effect of the shape of the inverse star point (point A of Fig. 1) on the stress at the star point. The purpose of determining this effect was twofold: (1) so the designer would know whether the results presented herein were applicable to the grain in question and (2) to give him an indication of the effect on the stress at the star point caused by minor variations of the internal geometry that might be imposed for ballistic reasons.

Two types of tests were conducted. The first and most significant was to vary a' while the remainder of the geometry was held constant. The initial point on each curve is at a value of a'/a that corresponds to the pointed inverse star point. This condition has the relationship

$$\frac{a'}{a} = \frac{\rho}{a} \csc \frac{\pi}{N}$$

(Smaller values of a'/a do not correspond to a possible star configuration.)

The tests were made by machining a blank to the pointed inverse star configuration, testing it while it was being subjected to external pressure, and then remachining it to increase a'/a. The specimen was tested and the process repeated. Because the configuration remained the same in the region near the star point where the maximum stress was being determined, a fresh edge was not produced there before each test; hence, the time-edge effect must be accounted for. The solid curves of Fig. 11 are based on the uncorrected test data; the dashed curves represent data that have been corrected for time-edge effect by using some recently obtained (tentative) correction factors. At this time, there are insufficient data to decide between these curves. However, the true effect is undoubtedly bracketed by the corrected and uncorrected curves.

The second type of test was run to check results presented by Wilson (Ref. 3 and 4) for an analytic solution that will be discussed later in this report, and to check the effect of changing the entire character of the internal boundary. In these tests, the internal boundary was made to correspond to Wilson's geometry as closely as conveniently possible. This resulted in a square hole rather than the normally circular one. The results of these tests were not significantly different from those of an inscribed circular hole.

PROCESSING OF TEST DATA

The pressure-loading tests were made by noting the pressure at which each fringe appeared at the point where stress was to be determined. In the thick-walled hollow cylinder, the fringes were rather broad rings, which made an accurate determination of the location of the fringe difficult. In most cases, only four fringes could be observed because of a 400-psi equipment limitation on the pressure. The combination of indistinct fringes and four or five data points makes the determination of dp_0/dn (and thus $d\sigma_0/dp_0$) difficult. Typical data points can be observed in Fig. 12. In contrast, the star configuration exhibits a very sharp fringe pattern: eight to ten fringes can be observed without exceeding $p_0 = 400$ psi. Also, these eight to ten data points were obtained for at least three star points on every configuration, giving three sets of test points from which the slope dp_0/dn could be determined. Typical data are shown in Fig. 13.

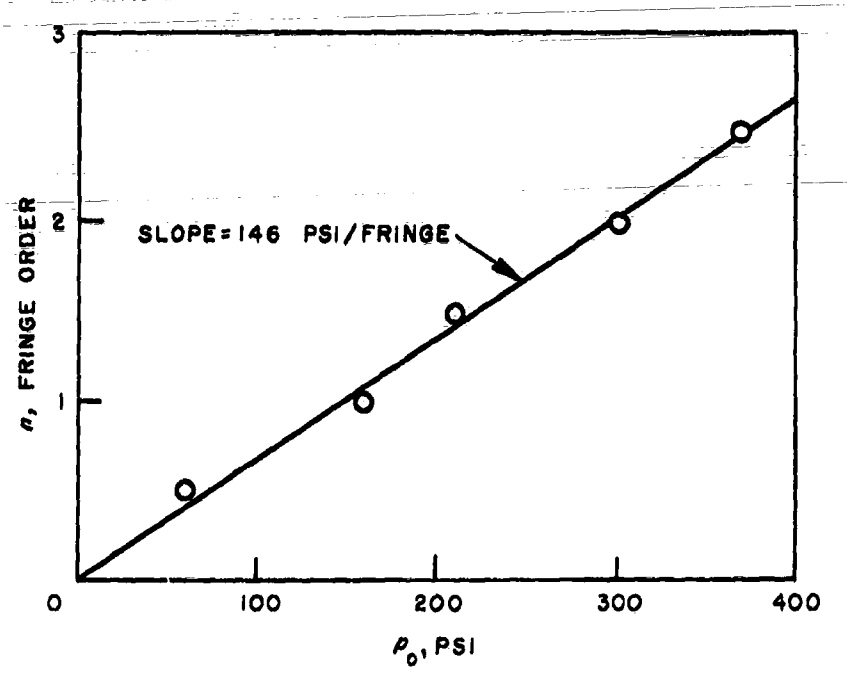

FIG. 12. Fringe Order Versus Pressure for an Externally Pressurized Thick-Walled Hollow Cylinder of CR-39 Plastic; $a/b = 0.368$; $h = 0.253$.

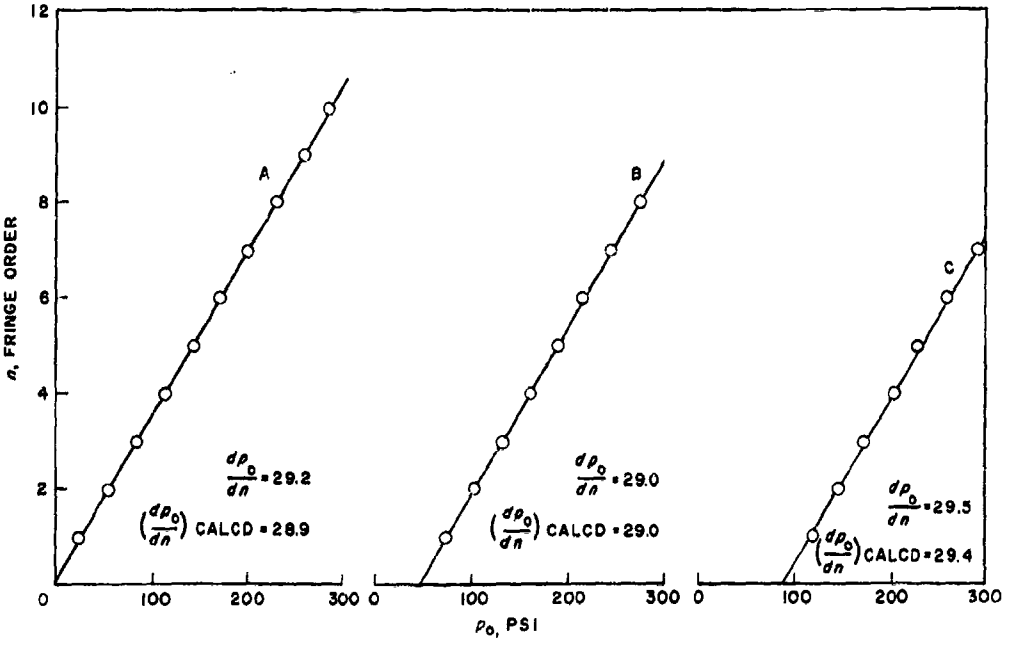

FIG. 13. Fringe-Order-Versus-Pressure Curves for Three Star Points (A, B, C) of an Externally Pressurized Six-Point-Star Grain.

The data from each test were plotted in the p_0 versus n plane, and the best straight line (visually) was plotted through the data. The slope of this line was read from the plot. A calculation method was also used that determined the slope of the straight line through the data points by minimizing the sum of the squares of the distance of the data points from the line (Ref. 5).

The slope determined in this manner was compared to the visually determined slope. It soon became apparent that the least-square-calculated slopes yielded data of slightly greater internal consistency. The scheme also eliminated the human element and provided a standard way of defining the "best slope." Ultimately, the plotted data became simply a check against wild (misread) data points or calculation errors. The calculated values of slope were used for all subsequent plotting and calculation and are denoted by (dp_0/dn)calcd.

In view of the more accurately determined slopes dp_0/dn for the star configuration, it is clear that the curves determined from these data must compare to the unknown theoretical values at least as well as the poorer thick-walled-cylinder calibration data compare to the known theoretical curves, as shown in Fig. 5.

A total of 34 data points on the $d\sigma_\theta/dp_0$ versus w/ρ and w/b curves was obtained for the six-point-star configuration, which was chosen as the control on which the most extensive work would be done. In addition, a limit point was known on each curve of constant w/b when plotted versus w/ρ. Consider the situation when w and b are held constant and $w/\rho \to 0$. It is clear that this process implies $\rho \to \infty$. However, a moment's reflection on the geometry indicates that the star configuration ceases to exist for $\rho > a$ and that the case $\rho = a$ reduces to a thick-walled cylinder. σ_θ/p_0 for this cylinder can be calculated from Eq. 5, and represents the limit point (shown as crosshatched areas in Fig. 6–10) on the curves as $w/\rho \to 0$. With these limit points plus four experimental points on each curve, the shapes of the curves of constant w/b in the σ_θ/p_0 versus w/ρ plane were quite well defined.

For the three-, four-, five-, and eight-point star configurations, a total of 50 tests was run. The limit point, the two data points on each of these curves, and the known shape of the curve from the six-point star data were sufficient to define the curves for these configurations. Crossplots of various parameters versus N were also constructed from the initial curves and used to smooth the σ_θ/p_0 versus w/ρ curves. An example of a crossplot is given in Fig. 14.

ERROR IN EXPERIMENTAL RESULTS

The final results are given in the form σ_θ/p_0 versus w/ρ along curves of constant w/b. The location of a given experimental data point in the σ_θ/p_0 versus w/ρ plane is determined by these three values.

As has been previously pointed out, machining errors resulting in inaccurate geometry are entirely negligible; therefore, the point may be assumed to be perfectly located with respect to the two parameters that depend only on geometry $(w/\rho, w/b)$. Thus, the error of location of an experimental point reduces to an evaluation of the error in determining σ_θ/p_0. In Eq. 2, the relative error in σ_θ/p_0 is the sum of the relative errors in $2f/h = F(0.250)/h$ and in dp_0/dn. From Fig. 4 it may be seen that the error in F is within $\pm 0.5\%$. The thickness of each specimen, h, was measured with a micrometer. The thickness was nominally 0.250 inch, and readings were taken to the nearest 0.001 inch. However, the thickness tended to vary over a given specimen, so the average value was used in calculations. Specimens with a variation of more than ± 0.003 inch were rejected. Using the average value of h under these circumstances certainly could not introduce an error of over $0.003/0.250 \times 100\% = 1.2\%$. However, the expected error would be considerably less than this, and $\pm 0.5\%$ represents a conservative estimate. Thus, the total contribution to error from f/h is $\pm 1\%$.

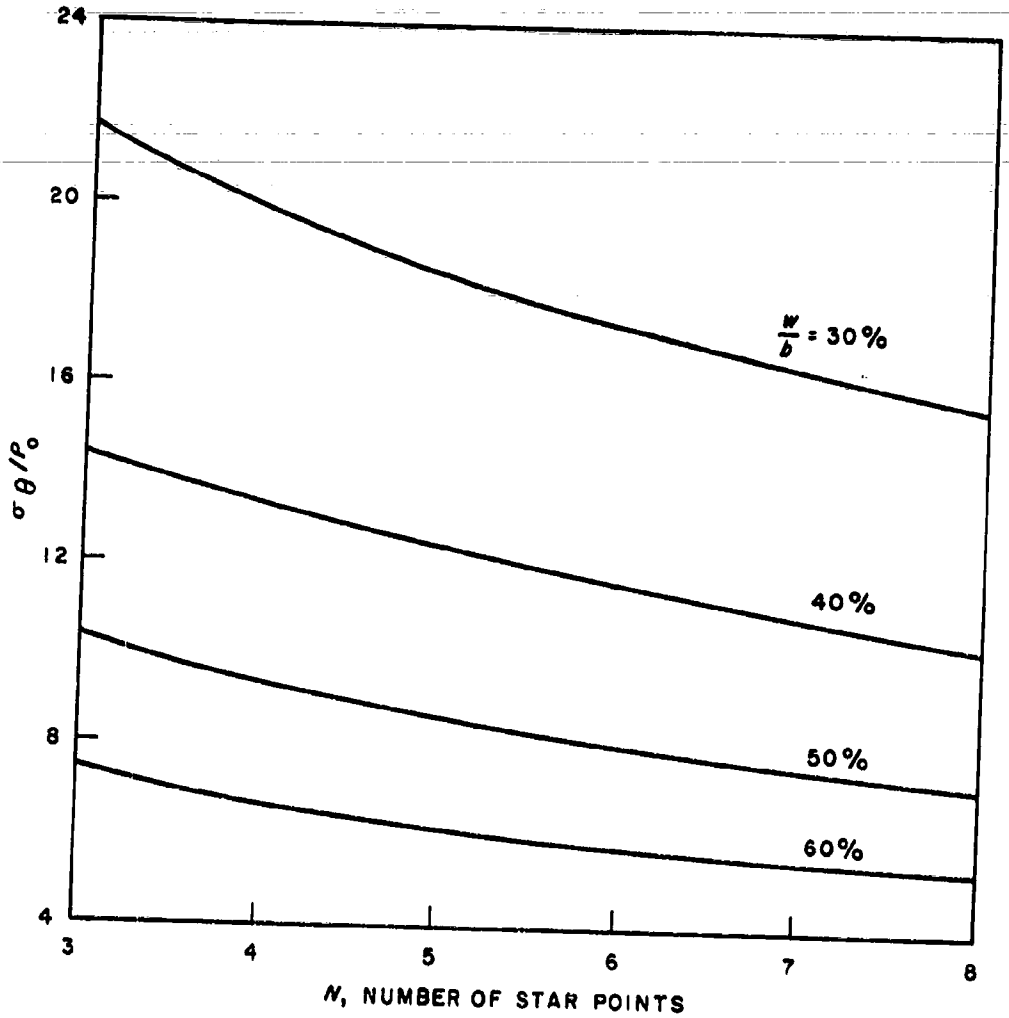

FIG. 14. Effect of Number of Star Points on the Stress at the Star Point; $w/\rho = 16.0$.

The relative-error contribution from dp_0/dn is more difficult to estimate. The pressure was read from a calibrated gage, so the error from this source is negligible. Eight to ten data points were used to determine each straight-line curve, and three independent curves were taken from each specimen. The internal consistency of the data is excellent (Fig. 13).

A maximum of ±3% relative error in the (averaged over three-star-point) dp_0/dn data appears reasonable because of internal evidence (consistency of data) and external evidence (comparison with thick-walled-cylinder data gathered under test conditions identical to those for the known theoretical values (Fig. 5), bearing in mind the inherently poorer internal consistency of the thick-walled-cylinder data (compare Fig. 12 and 13)).

Thus, each experimental point on the curves should be within ±4% of the correct value. The best smoothed curves are shown, with the actual test points indicated, in Fig. 6–10. If the curves are assumed to be continuous, monotonic, and reasonably smooth with respect to all variables,

then the final curves probably fall well within ±4% of the true values over most of the range of engineering interest.

COMPARISON WITH A THEORETICAL SOLUTION

Wilson (Ref. 3 and 4) determined the stress in a four-point-star grain analytically by means of a complex-variable approach. In this analysis, he uses a four-term transformation that transforms a circle into a shape matching the shape of the grains tested herein in two parameters: namely, positions of star points and radius of curvature at the star point. The over-all shape, however, is somewhat different, particularly in regions away from the star point. Fortunately, the effect of these regions on the maximum stress at the star point is negligible (Fig. 11).

The results of the experimental test for a configuration similar to that of Ref. 4 are shown in Fig. 15, which gives a direct comparison of the two solutions over the common range. As may be seen, the agreement is excellent; the values of the test data are at most 2% higher than the theoretical.

EXTENSION OF TEST DATA

STRESS-CONCENTRATION FACTORS

Although the results presented thus far are for a grain subjected only to external pressure, the results may be extended to several other cases of practical interest.

Free Grain With Internal Pressure. For a grain that is unloaded at the outer boundary but subjected to an internal pressure, p_i, the use of Eq. 1 and 2 putting $\sigma_1 = \sigma_\theta$ and $\sigma_2 = -p_i$ gives

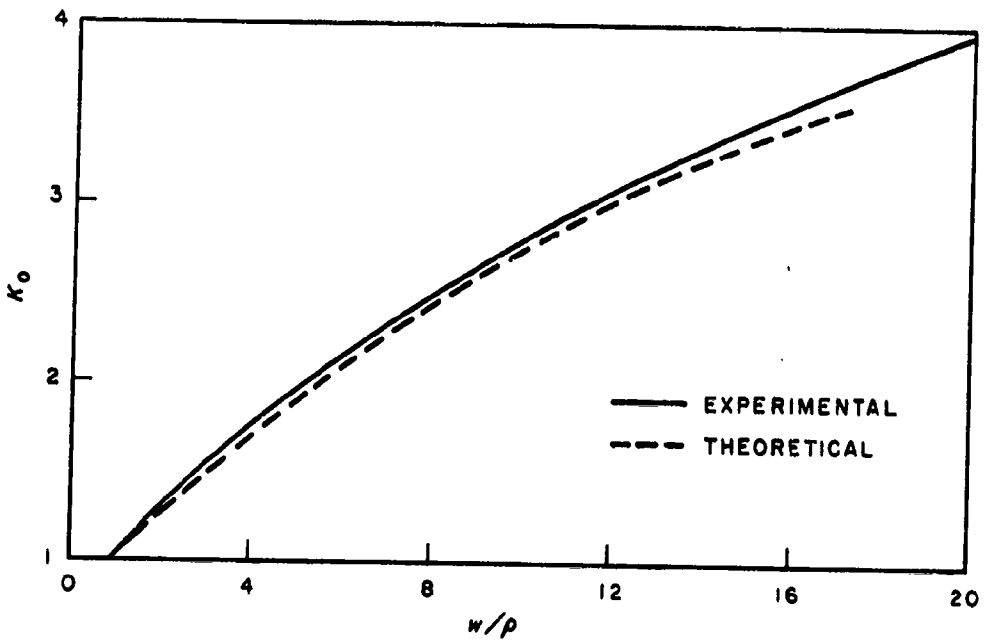

FIG. 15. Comparison of Theoretical and Experimental Stress-Concentration Factors for an Externally Pressurized Four-Point-Star Grain; $a/b = 0.5$.

$$\frac{\sigma_\theta}{p_i} = \frac{2f/h}{dp_i/dn} - 1$$

or, because $(2f/h)/(dp_i/dn)$ is formally equivalent to the value σ_θ/p_0 in Fig. 6–10,

$$\frac{\sigma_\theta}{p_i} = \frac{\sigma_\theta}{p_0} - 1 \tag{6}$$

Hence, the stress at the star point caused by an internal pressure, p_i, may be determined immediately by reading the value of σ_θ/p_0 off the graphs at the appropriate values of the geometric parameters and using Eq. 6.

Case-Bonded Grain With Internal Pressure. For a case-bonded configuration, it is convenient, although not necessary, to introduce the concentration factor defined in Ref. 2 as

$$K_i = \frac{\sigma_1 - \sigma_2}{\bar{\sigma}_1 - \bar{\sigma}_2} \tag{7}$$

where the barred quantities refer to the stress in a corresponding thick-walled cylinder. For the case in question,

$$\bar{\sigma}_1 - \bar{\sigma}_2 = \bar{\sigma}_r - \bar{\sigma}_\theta = \frac{2(p_0 - p_i)}{1 - (a/b)^2} \tag{8}$$

The factor $2/[1 - (a/b)^2]$ has been plotted versus w/b in Fig. 16. Therefore, the concentration factor may be determined immediately from the expression

$$K_i = \frac{\sigma_\theta/p_0}{2/[1 - (a/b)^2]} \tag{9}$$

The value of σ_θ/p_0 is obtained from Fig. 6–10. It is of interest to note that the expression

$$\frac{\sigma_\theta}{p_0} = \frac{2K_i}{1 - (a/b)^2} \tag{10}$$

holds for all the expressions that follow. Hence, as indicated above, the introduction of the stress-concentration factor is not necessary, but was done so that results quoted herein might be compared with earlier data.

In actual practice, the grain will be restrained by a relatively rigid case. As stated previously, it has been found satisfactory for engineering accuracy to replace the effect of the case enclosing an internally pressurized star grain by p', a uniformly distributed interface pressure.[3] If the thickness of the case is assumed small, the interface pressure is given by

$$p' = \frac{2p_i}{1 + \nu + (1 - \nu)\left(\frac{b}{a}\right)^2 + \left[\left(\frac{b}{a}\right)^2 - 1\right]\frac{Eb}{E_c h_c}} \quad \text{(plane stress)} \tag{11}$$

$$p' = \frac{2(1 - \nu)p_i}{\left[1 + (1 - 2\nu)\left(\frac{b}{a}\right)^2\right] + \left[\left(\frac{b}{a}\right)^2 - 1\right]\frac{1 - \nu_c^2}{1 + \nu} \cdot \frac{Eb}{E_c h_c}} \quad \text{(plane strain)} \tag{12}$$

[3] The actual interface pressure caused by internal pressurization varies because of the irregular shape of the star grain. This variation is well approximated by a sinusoidally varying pressure applied at the outer boundary. However, the authors in unpublished experiments have found that the effect of this variation on the stress at the star point is small.

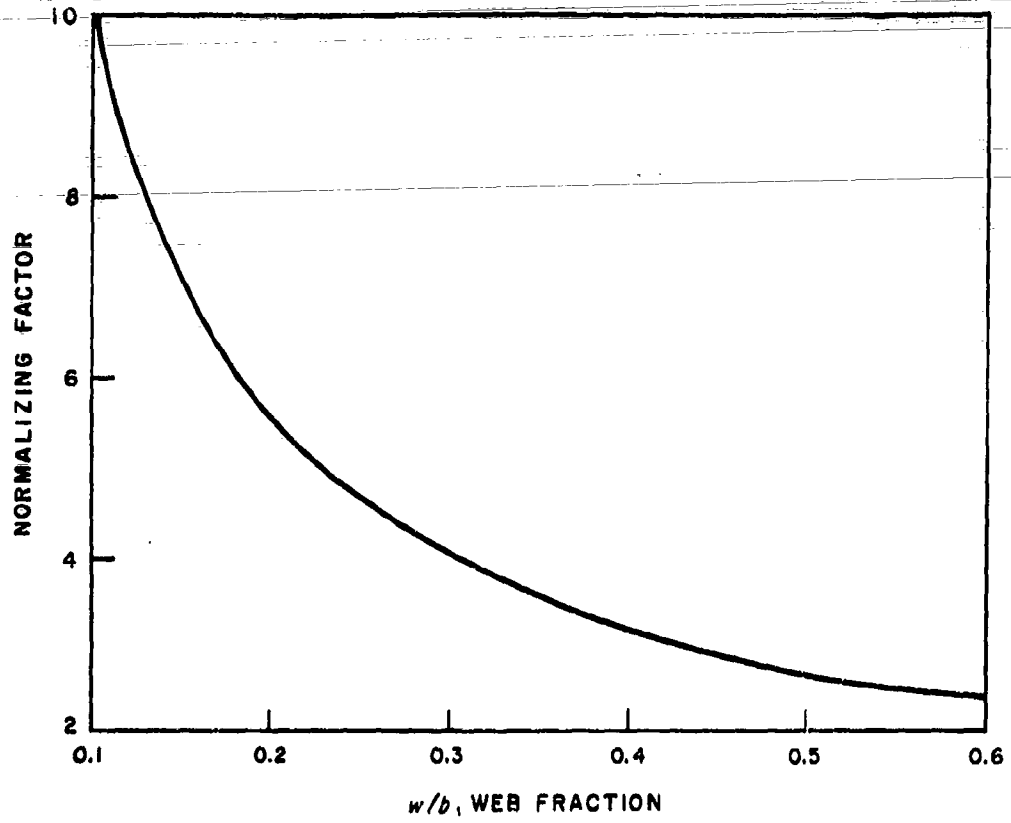

FIG. 16. Variation of Normalizing Factor With Web Fraction.

where h_c is the thickness of the case and the subscript c on other quantities refers to the case. From Eq. 7,

$$\sigma_r - \sigma_\theta = K_i(\bar{\sigma}_r - \bar{\sigma}_\theta) \tag{13}$$

The normalizing stress is given by Eq. 8 and 11 or 12, whichever is applic[illegible] at the inner surface is $-p_i$. Inserting these values in Eq. 13, and for simplicity ass[illegible] compressible grain ($\nu = 1/2$) and a state of plane strain, the expression for the tangential stress becomes

$$\frac{\sigma_\theta}{p_i} = \frac{2K_i}{1-\left(\frac{a}{b}\right)^2}\left\{1 - \frac{1}{1+\frac{2}{3}\left[\left(\frac{b}{a}\right)^2 - 1\right](1-\nu_c^2)\frac{Eb}{E_c h_c}}\right\} - 1 \tag{14}$$

or, using Eq. 10,

$$\frac{\sigma_\theta}{p_i} = \frac{\sigma_\theta}{p_0}\left\{1 - \frac{1}{1+\frac{2}{3}\left[\left(\frac{b}{a}\right)^2 - 1\right](1-\nu_c^2)\frac{Eb}{E_c h_c}}\right\} - 1 \tag{15}$$

Hence, the stress under such a loading condition is determined from the expressions above, and the value of σ_θ/p_0 is obtained from Fig. 6–10.

STRAIN-CONCENTRATION FACTORS

Strain-concentration factors may also be calculated from the information contained in this report. The stress–strain relationships in cylindrical coordinates for a state of plane strains are given by

$$\epsilon_r = \alpha(\sigma_r + \beta\sigma_\theta) \tag{16}$$

$$\epsilon_\theta = \alpha(\sigma_\theta + \beta\sigma_r) \tag{17}$$

$$\gamma_{r\theta} = (1/G)\tau_{r\theta} \tag{18}$$

where

$$\alpha = \frac{1 - \nu^2}{E}, \qquad \beta = \frac{\nu}{\nu - 1} \tag{19}$$

A strain-concentration factor may be defined in a manner similar to the stress-concentration factor, i.e.,

$$K_\epsilon = \frac{\epsilon_1 - \epsilon_2}{\bar{\epsilon}_1 - \bar{\epsilon}_2} \tag{20}$$

where ϵ_1 and ϵ_2 are the principal strains, and the barred quantities denote the strains in a thick-walled hollow cylinder. In an isotropic elastic material, the directions of principal stress and strain coincide; hence, along the line of symmetry where there is no shearing strain, Eq. 20 may be written as

$$K_\epsilon = \frac{\epsilon_r - \epsilon_\theta}{\bar{\epsilon}_r - \bar{\epsilon}_\theta} \tag{21}$$

Using Eq. 16 and 17, the difference in principal strain may be written as

$$\epsilon_r - \epsilon_\theta = \alpha(\beta - 1)(\sigma_\theta - \sigma_r) \tag{22}$$

Hence, as would be expected, the difference in principal strains is a function only of the difference in principal stress, which in turn depends only on pressure difference. This fact allows any statements or proofs concerning the relationship of the fringe pattern resulting from internal or external pressure in the stress problem to be applied directly to the strain problem.

Now, for the specific problem under consideration: namely, internal pressurization of a case-bonded grain,

$$\begin{gathered} \sigma_r = -p_i \\ \sigma_\theta = \frac{2K_i}{1 - (a/b)^2}(1 - P)(p_i) - p_i \\ \alpha(\beta - 1) = -\left(\frac{1 + \nu}{E}\right) \\ P = \frac{p'}{p_i} \end{gathered} \tag{23}$$

For the normalizing cylinder, all quantities are the same with the exception of the concentration factor, which is unity. Combining the expressions of Eq. 23 in Eq. 22 gives

$$\epsilon_r - \epsilon_\theta = \frac{1 + \nu}{E} \cdot \frac{2K_i}{1 - (a/b)^2}(P - 1)p_i \tag{24}$$

hence

$$K_\epsilon = \frac{\epsilon_r - \epsilon_\theta}{\bar{\epsilon}_r - \bar{\epsilon}_\theta} = K_i \tag{25}$$

That is, the numerical value of the strain-concentration factor as defined above for an internally pressurized grain is identical to the stress-concentration factor for a free grain subjected to external pressure.

It is important for the designer to note that the radial component of the strain does not vanish at the star point. In the case of the stress-concentration factor, the radial stress was either zero or the negative of the internally applied pressure; in any event, the radial stress was specified independently of the tangential stress. Examination of Eq. 16 reveals that this is not true for the strain-concentration factor. There is a contribution to the radial strain from both the tangential and radial stresses. It is possible that the tangential strain or the ratio of the tangential strains to the normalizing tangential strains might become quite large compared to the strain-concentration factor defined above. Hence, the designer must decide which parameter is important in the failure of a grain and compute the concentration factor from the data presented accordingly. The fundamental importance of establishing an appropriate failure criterion has been strongly emphasized (Ref. 2).

The extensions presented above do not exhaust the list of possible ones that can be made from the data given herein. Indeed, extensions to certain thermal-stress situations have been pointed out (Ref. 1 and 6). Finally, these data do not cover all configurations of ballistic interest, but it is believed that this parametric study of one set of typical geometries will help the designer at least to estimate the factors for his specific problem.

CONCLUSIONS

Photoelastic tests were conducted to determine the maximum tangential stress for a family of star-grain configurations. Curves are presented that give the value of this parameter for web fractions from 20 to 60%, for w/ρ from approximately 2 to 30 (where w is the web thickness of the grain, and ρ is the radius of the star point), and for N (number of star points) from 3 to 8. The curves are expected to be accurate to ±4% over the range tested.

The effect of the inverse star point was investigated and found to be negligible over a range of shapes and values of the parameter a'/a from approximately zero to 0.6. The experimental results are compared to one known theoretical calculation, and the agreement is found to be excellent.

Appendix
DERIVATION OF EMPIRICAL EQUATION

The results of the tests described in the body of this report are presented in Fig. 6–10. It is the purpose of this appendix to show the derivation of an empirical equation that represents these experimental data. The equation derived gives the ratio of tangential stress to external pressure as an explicit function of the three controlling parameters: web fraction, radius of the star point, and number of star points. The ranges of these parameters are as follows: web fractions, from 20 to 60%; w/ρ, from 2 to 30 (where w is the web thickness of the grain and ρ is the radius of the star point); and N (number of star points), from 3 to 8. The accuracy of the equation was demonstrated, and good agreement with the experimental data was achieved.

The main reason for obtaining an explicit algebraic relationship for the stress as a function of the various parameters is that such a relationship may be used directly in ballistic calculations. Previously it was necessary to arrive at a configuration for a specific ballistic requirement by an iterative process. In such a process, a geometry is first selected without regard to the stress level involved. This configuration is then tested, and the results obtained are used to judge the relative merit of the design from the stress standpoint. However, with the equation presented and by the use of a high-speed computer, it is possible to introduce stress considerations directly into the selection process. In principle, for a given ballistic mission, the minimum stress configuration of a family of grains could be determined purely by machine computation.

METHOD OF CURVE FITTING

The nature of the experimental curves presented in Fig. 6–10 and crossplots such as Fig. 14 suggest that the data may be represented by a function of the form

$$\sigma_\theta/p_0 = N^k \Phi(w/b, w/\rho) \tag{26}$$

If w/b and w/ρ are held constant (i.e., the function Φ), the value of k may be obtained from the experimental curves. By the application of this procedure, the assumption that k is independent of w/b and w/ρ was verified, except in a limited region near the limit point

$$\frac{w}{\rho} \to \frac{w/b}{1-(w/b)}$$

The value of k thus determined is -0.34.

Knowing the dependence of the curves on N, the functional nature of Φ was determined from the curves for a specific value of N. The curves for $N = 6$ were chosen for this purpose. The shape of these curves suggested choosing

$$\Phi(w/b, w/\rho) = \alpha(w/b)\cdot(w/\rho)^{\beta(w/b)} + \gamma(w/b) \tag{27}$$

or

$$\log(\Phi - \gamma) = \beta \log(w/\rho) + \log \alpha \tag{28}$$

For fixed w/b(20%, 30%, . . . , 60%), Eq. 28 gives the relationship between the experimentally known $\Phi(w/\rho)$ and the constants α and β. The right-hand side is the equation of a straight line

in the log log plane, with slope β and intercept α. By choosing several values of γ, it was possible to make the experimentally determined data (left-hand side) also plot as a straight line in the log log plane, thus showing that the assumed form for the function Φ is an appropriate one. The γ that makes the experimental data plot as a straight line and the α and β determined from this straight line were then known for each value of w/b. α, β, and γ were plotted as a function of w/b, and appropriate functions were fitted to the curves so defined. In this manner, the following functions were determined

$$\begin{aligned} \alpha &= 0.52\,(w/b)^{-1.77} - 0.80 \\ \beta &= 1.90\,(w/b)^{0.175} - 1.0 \\ \gamma &= 1.7\{1 - 15.8\,\exp\,[-18.4\,(w/b)]\} \end{aligned} \tag{29}$$

The empirical function thus obtained is

$$\sigma_\theta/p_0 = (6/N)^{0.34}\Big([0.52(w/b)^{-1.77} - 0.80](w/\rho)^{[1.90(w/b)^{0.175}-1.0]} + 1.7\{1 - 15.8\,\exp\,[-18.4(w/b)]\}\Big) \tag{30}$$

This function holds over the region of the experimental data, but fails near the limit point

$$\frac{w}{\rho} \to \frac{w/b}{1-(w/b)}$$

Near this point, the value of σ_θ/p_0 approaches the value for a thick-walled cylinder, and, thus, σ_θ/p_0 is independent of N. To extend the validity of Eq. 30 to this limit region, the term describing the N dependence was modified in the following manner: a function was devised that tended to $(6/N)^{0.34}$ for

$$\frac{w}{\rho} \gg \frac{w/b}{1-(w/b)}$$

and tended to 1 as w/ρ tended to

$$\frac{w/b}{1-(w/b)}$$

A satisfactory function, which provides a smooth transition for the N dependence of this nature, is

$$1 + \left[\left(\frac{6}{N}\right)^{0.34} - 1\right]\left(1 - \exp\left\{-0.4\left[\frac{w}{\rho} - \frac{w/b}{1-(w/b)}\right]\frac{b}{w}\right\}\right) \tag{31}$$

Hence, in any problem in which the value of σ_θ/p_0 near the limit point is required, the following expressions should be used instead of Eq. 30.

$$\frac{\sigma_\theta}{p_0} = \left[1 + \left[\left(\frac{6}{N}\right)^{0.34} - 1\right]\left(1 - \exp\left\{-0.4\left[\frac{w}{\rho} - \frac{w/b}{1-(w/b)}\right]\frac{b}{w}\right\}\right)\right] \cdot \left\{\left[0.52\left(\frac{w}{b}\right)^{-1.77} - 0.80\right]\left(\frac{w}{\rho}\right)^{[1.90(w/b)^{0.175}-1.0]} + 1.7\left[1 - 15.8\,\exp\left(18.4\,\frac{w}{b}\right)\right]\right\} \tag{32}$$

It should be noted that for normal usage, the range covered by Eq. 30 will be sufficient.

ACCURACY OF RESULTS

Values of σ_θ/p_0 given by Eq. 32 in the region of the experimental data were calculated. Curves were drawn through these points and superimposed on the experimental curves. Curves for the three-point-star grain are shown in Fig. 17. It will be observed that the agreement is excellent, with discrepancies of less than 5% over most of the range of interest. The maximum deviation occurs on the three-point-star curve for w/b of 40%. This single point deviates from the experimental one by 11%. It should be recalled that the accuracy of this curve was quoted as ±4%; hence, agreement might range between 7 and 15%. While the error of this single curve at first observation appears large, it must be viewed in the light of the excellent agreement of the empirical equation with the remainder of the data and the fact that this curve was determined by only two data points. This discrepancy could easily be corrected by adding yet another factor to Eq. 32. However, because of the over-all agreement with the remainder of the data, the additional complication involved was not considered justified.

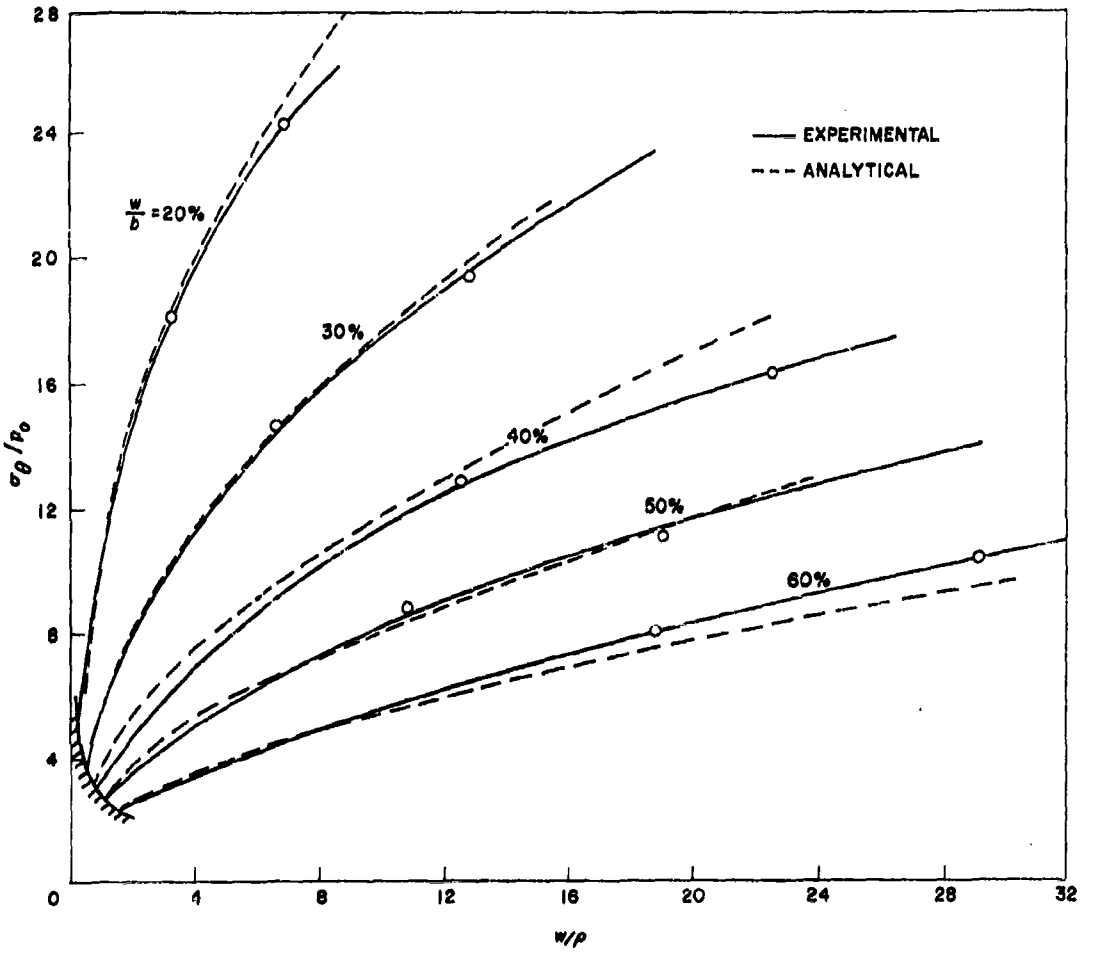

FIG. 17. Comparison of Experimental and Analytical Curves for the Three-Point-Star Grain.

REFERENCES

1. Ordahl, D. D., and M. L. Williams. "Preliminary Photoelastic Design Data for Stresses in Rocket Grains," Jet Propulsion, Vol. 27, No. 6 (June 1957), pp. 657–62.
2. Guggenheim Aeronautical Laboratory, California Institute of Technology. Fundamental Studies Relating to Systems Analysis of Solid Propellants, by M. L. Williams, P. J. Blatz, and R. A. Schapery. Pasadena, Calif., CIT, February 1961, 295 pp. (GALCIT SM 61-5.)
3. Rohm & Haas Co. "An Analysis of the Stresses and Displacements Due to Internal Pressure in a Case-Bonded Solid-Propellant Grain With a Four-Pointed Star-Shaped Internal Perforation," by H. B. Wilson, Jr., Quarterly Progress Report on Engineering Research (U), March 15, 1960 to June 15, 1960. Huntsville, Ala., Rohm & Haas Co., 10 July 1960. 33 pp. (Report No. P-60-11.)
4. Wilson, Howard B., Jr. "Stresses Owing to Internal Pressure in Solid Propellant Rocket Grains," ARS Journal, Vol. 31, No. 3 (March 1961), pp. 309–17.
5. Reddick, H. W., and F. H. Miller. Advanced Mathematics for Engineers. New York, Wiley, 1938, p. 387.
6. Cox, W. T. "Comment on 'Stresses in Rocket Grains'," Jet Propulsion, Vol. 28, No. 5 (May 1958), p. 342.

INITIAL DISTRIBUTION

14 Chief, Bureau of Naval Weapons
- DLI-31 (2)
- FWEW (1)
- RM (1)
- RM-1 (1)
- RM-3 (1)
- RM-35 (1)
- RMMP (1)
- RRMP-12 (1)
- RMMP-4 (1)
- RRRE-5 (1)
- RRRE-6 (1)
- RRRE-21 (1)
- RT-11 (1)

1 Special Projects Office (Solid Propellants Section)
1 Chief of Naval Research (Mechanics Branch, J. M. Crowley)
1 Naval Ordnance Laboratory, White Oak (WC)
3 Naval Propellant Plant, Indian Head
- Code P (2)
- Code R (1)

2 Naval Weapons Services Office, Naval Weapons Plant
1 Bureau of Naval Weapons Resident Representative, Sacramento
1 Chief of Ordnance (ORDTU)
1 Aberdeen Proving Ground (Internal Ballistics Laboratory)
4 Army Rocket & Guided Missile Agency, Redstone Arsenal (Technical Library, ORDXR-OTL)
1 Office of Ordnance Research, Durham (Dr. James Murray)
2 Picatinny Arsenal (Library)
1 White Sands Proving Ground (Technical Librarian)
1 Headquarters, U. S. Air Force
1 Air Force Ballistic Missile Division, Los Angeles (WDSIT-7-162)
2 Air Force Flight Test Center, Edwards Air Force Base (D. A. Hart)
1 Air Force Office of Scientific Research (Mechanics Division)
1 Air Research and Development Command, European Office, Brussels (Library, Technical Information Office)
1 Air Proving Ground Center, Eglin Air Force Base (PGTRI)
1 Ogden Materiel Area, Hill Air Force Base (OOMQQC/Lt. Graham/3644)
1 Tactical Air Command, Langley Air Force Base (TPL-RQD-M)
1 Aeronautical Systems Division, Wright-Patterson Air Force Base (ASAPRD-DIST)
1 Advanced Research Projects Agency (John Kincaid)
10 Armed Services Technical Information Agency (TIPCR)
1 Director of Defense (R&E) (William E. Sheehan)
1 Lewis Research Center (George Mandel)
2 National Aeronautics & Space Administration
- Elliott Mitchell (1)
- R. W. Ziem (1)

4 British Joint Services Mission, Ministry of Supply Staff (Reports Officer), via BuWeps (DSC)
4 Defence Research Member, Canadian Joint Staff (W), via BuWeps (DSC)

ABSTRACT CARD

U. S. Naval Ordnance Test Station

Stress-Concentration Data for Internally Perforated Star Grains, by M. E. Fourney and R. R. Parmerter of the Mathematical Sciences Corporation. China Lake, Calif., NOTS, December 1961. 24 pp. (NAVWEPS Report 7758, NOTS TP 2728), UNCLASSIFIED.

ABSTRACT. Completing preliminary work initiated by NOTS several years ago, photoelastic tests were conducted to determine the maximum tangential stress for a family of star-grain configurations in a state of plane stress. Curves are presented that give the value of the ratio of tangential stress to external pressure for web fractions from 20 to 60%,

(Over)
1 card, 4 copies

U. S. Naval Ordnance Test Station

Stress-Concentration Data for Internally Perforated Star Grains, by M. E. Fourney and R. R. Parmerter of the Mathematical Sciences Corporation. China Lake, Calif., NOTS, December 1961. 24 pp. (NAVWEPS Report 7758, NOTS TP 2728), UNCLASSIFIED.

ABSTRACT. Completing preliminary work initiated by NOTS several years ago, photoelastic tests were conducted to determine the maximum tangential stress for a family of star-grain configurations in a state of plane stress. Curves are presented that give the value of the ratio of tangential stress to external pressure for web fractions from 20 to 60%,

(Over)
1 card, 4 copies

U. S. Naval Ordnance Test Station

Stress-Concentration Data for Internally Perforated Star Grains, by M. E. Fourney and R. R. Parmerter of the Mathematical Sciences Corporation. China Lake, Calif., NOTS, December 1961. 24 pp. (NAVWEPS Report 7758, NOTS TP 2728), UNCLASSIFIED.

ABSTRACT. Completing preliminary work initiated by NOTS several years ago, photoelastic tests were conducted to determine the maximum tangential stress for a family of star-grain configurations in a state of plane stress. Curves are presented that give the value of the ratio of tangential stress to external pressure for web fractions from 20 to 60%,

(Over)
1 card, 4 copies

U. S. Naval Ordnance Test Station

Stress-Concentration Data for Internally Perforated Star Grains, by M. E. Fourney and R. R. Parmerter of the Mathematical Sciences Corporation. China Lake, Calif., NOTS, December 1961. 24 pp. (NAVWEPS Report 7758, NOTS TP 2728), UNCLASSIFIED.

ABSTRACT. Completing preliminary work initiated by NOTS several years ago, photoelastic tests were conducted to determine the maximum tangential stress for a family of star-grain configurations in a state of plane stress. Curves are presented that give the value of the ratio of tangential stress to external pressure for web fractions from 20 to 60%,

(Over)
1 card, 4 copies

for w/ρ from approximately 2 to 30 (w is the web thickness of the grain, and ρ is the radius of the star point), and for N (number of star points) from 3 to 8. The accuracy of the curves is estimated to be within $\pm 4\%$. The effect of the inverse star point was investigated and found to be negligible over a range of shapes and values of the parameter a'/a (ratio of distances from center to the inverse star point and to the outer star point) from approximately zero to 0.6. The experimental results compared favorably with one theoretical calculation. Equations are given for extension of the data to case-bonded, internally pressurized grains and for application to problems of tangential strain. An appendix presents an empirical equation representing the data.

NAVWEPS Report 7758

for w/ρ from approximately 2 to 30 (w is the web thickness of the grain, and ρ is the radius of the star point), and for N (number of star points) from 3 to 8. The accuracy of the curves is estimated to be within $\pm 4\%$. The effect of the inverse star point was investigated and found to be negligible over a range of shapes and values of the parameter a'/a (ratio of distances from center to the inverse star point and to the outer star point) from approximately zero to 0.6. The experimental results compared favorably with one theoretical calculation. Equations are given for extension of the data to case-bonded, internally pressurized grains and for application to problems of tangential strain. An appendix presents an empirical equation representing the data.

NAVWEPS Report 7758

for w/ρ from approximately 2 to 30 (w is the web thickness of the grain, and ρ is the radius of the star point), and for N (number of star points) from 3 to 8. The accuracy of the curves is estimated to be within $\pm 4\%$. The effect of the inverse star point was investigated and found to be negligible over a range of shapes and values of the parameter a'/a (ratio of distances from center to the inverse star point and to the outer star point) from approximately zero to 0.6. The experimental results compared favorably with one theoretical calculation. Equations are given for extension of the data to case-bonded, internally pressurized grains and for application to problems of tangential strain. An appendix presents an empirical equation representing the data.

NAVWEPS Report 7758

for w/ρ from approximately 2 to 30 (w is the web thickness of the grain, and ρ is the radius of the star point), and for N (number of star points) from 3 to 8. The accuracy of the curves is estimated to be within $\pm 4\%$. The effect of the inverse star point was investigated and found to be negligible over a range of shapes and values of the parameter a'/a (ratio of distances from center to the inverse star point and to the outer star point) from approximately zero to 0.6. The experimental results compared favorably with one theoretical calculation. Equations are given for extension of the data to case-bonded, internally pressurized grains and for application to problems of tangential strain. An appendix presents an empirical equation representing the data.

1 Aerojet-General Corporation, Azusa, Calif. (Librarian), via BuWepsRep
1 Aerojet-General Corporation, Sacramento (Librarian), via BuWepsRRep
1 Allegany Ballistics Laboratory, Cumberland, Md. (Librarian)
1 Armour Research Foundation, Chicago (Document Librarian for Department M)
1 Arthur D. Little, Inc., Cambridge (W. H. Varley)
1 Astro-Rocket, Inc., Mesa, Ariz. (Dr. David A. Fletcher)
2 Atlantic Research Corporation, Alexandria, Va.
A. Rice (1)
Library (1)
1 Battelle Memorial Institute, Columbus, Ohio (Dr. J. H. Jackson)
2 Boeing Airplane Company, Seattle
Ed Czarnecki (1)
Len Hadlock (1)
1 Brigham Young University, Provo, Utah (W. H. Beebe)
1 Brown University, Providence, R. I. (Department of Applied Mathematics, Dr. E. H. Lee)
5 California Institute of Technology, Pasadena
Dr. M. L. Williams (1)
Dr. P. J. Blatz (1)
M. E. Fourney (1)
R. R. Parmerter (1)
GALCIT Library (1)
1 Canadian Arsenal Research and Development Establishment, Quebec (L. A. Dickinson) via BuWeps (DSC)
1 Catholic University of America (Dr. J. H. Baltrukonis)
1 Columbia University, New York (Department of Civil Engineering, Dr. A. M. Freudenthal)
1 Convair, San Diego (Engineering Librarian)
2 Douglas Aircraft Company, Inc., Santa Monica, Calif.
Engineering Library, Department A-260 (1)
Engineering Library, Department A2-260 (1)
1 E. I. du Pont de Nemours & Company, Inc., Wilmington (Assistant Director of Research)
2 Emerson Electric Manufacturing Company, St. Louis (Wing Leong)
1 Explosives Research and Development Establishment, Waltham Abbey, England (Dr. J. H. C. Vernon) via BuWeps (DSC)
2 Grand Central Rocket Company, Redlands, Calif.
J. E. Fitzgerald (1)
J. W. Jones (1)
1 Hercules Powder Company, Explosives Department, Wilmington (A. M. Ball)
1 Hughes Aircraft Company, Culver City, Calif. (Technical Library)
1 Illinois Institute of Technology, Chicago (Dr. A. J. Durelli)
2 Jet Propulsion Laboratory, CIT, Pasadena (Library)
1 Lockheed Aircraft Corporation, Burbank, Calif. (Structures Division, Jackson E. Wignot)
1 Lockheed Aircraft Corporation, Georgia Division (Sci-Information Center)
1 Lockheed Aircraft Corporation, Missiles and Space Division, Palo Alto, Calif. (Polaris Propulsion Department, 66-27, Polaris System Integration)
2 Massachusetts Institute of Technology, Cambridge
Department of Mechanical Engineering, Prof. Norman C. Dahl (1)
Prof. R. L. Bisplinghoff (1)
1 Material Technology, Inc., Natick, Mass. (Dr. R. G. Cheatham)
1 Minnesota Mining & Manufacturing Company, St. Paul (George E. Chutka)

2 New York University, College of Engineering
    Dr. George Gerard (1)
    Dr. Bernard W. Shaffer (1)
1 Olin Mathieson Chemical Corporation, Marion, Ill. (Internal Ballistics Section, Technical Library)
3 Polytechnic Institute of Brooklyn (Department of Aeronautical Engineering)
    Dr. J. M. Klosner (1)
    Dr. Radok (1)
    Prof. F. Pohle (1)
1 Poudreries Reunies de Belgique S. A., Brussels (Jean Vanderkerckhove) via BuWeps (DSC)
4 Purdue University, Lafayette, Ind.
    Dr. A. C. Eringen (1)
    Dr. G. Lianis (1)
    Dr. R. J. H. Bollard (1)
    Library (1)
1 Research Institute of National Defense, Stockholm (G. Lennart Magnusson) via BuWeps (DSC)
1 Rocket Power/Talco, Mesa, Ariz. (Library)
1 Rocketdyne, Canoga Park, Calif. (Librarian)
2 Rocketdyne, McGregor, Tex. (Library)
4 Rohm & Haas Company, Redstone Arsenal Research Division
    Dr. Al Ignatowski (1)
    C. H. Parr (2)
    Technical Library (1)
2 Solid Propellant Information Agency, Applied Physics Laboratory, JHU, Silver Spring (K. F. Ockert)
1 Southwest Research Institute, Department of Chemistry and Chemical Engineering, San Antonio (Dr. H. C. McKee)
2 Space Technology Laboratories, Inc., Los Angeles
2 Stanford Research Institute, Poulter Laboratories, Menlo, Calif.
    Dr. T. L. Smith (1)
    W. L. Dowler (1)
1 Standard Oil Company, Research Department, Whiting, Ind. (B. H. Shoemaker)
2 Thiokol Chemical Corporation, Elkton, Md. (Ernest Sizemore)
2 Thiokol Chemical Corporation, Bristol, Pa. (Don Mueller)
1 Thiokol Chemical Corporation, Redstone Division, Redstone Arsenal (Technical Library)
3 Thiokol Chemical Corporation, Utah Division, Brigham City
    C. S. Roberts, Jr. (2)
    John Bruggenman (1)
2 United Technology Corporation, Sunnyvale, Calif.
    Dr. R. A. Chase (1)
    Librarian (1)
1 University of Alabama, University (Dr. William D. Jordan)
2 University of California, Berkeley (Department of Engineering Science)
    Prof. Karl S. Pister (1)
    Prof. Paul M. Naghdi (1)
1 University of Florida, Gainesville (Dr. W. A. Nash)
2 University of Illinois
    Dr. H. B. Wilson (1)
    Dr. H. H. Hilton (1)